

Published in final edited form as:

AJNR Am J Neuroradiol. 2013 August ; 34(8): 1573–1578. doi:10.3174/ajnr.A3471.

High Angular Resolution Diffusion Imaging (HARDI) Probabilistic Tractography of the Auditory Radiation

Jeffrey I. Berman, Ph.D.^{1,2}, Matthew R. Lanza¹, Lisa Blaskey, Ph.D.¹, J. Christopher Edgar, Ph.D.^{1,2}, and Timothy P. L. Roberts, Ph.D.^{1,2}

¹ Children's Hospital of Philadelphia, Department of Radiology

² University of Pennsylvania, Department of Radiology

Abstract

Background and Purpose—The auditory radiation crosses other white matter tracks and cannot reliably be delineated or quantitatively assessed with DTI fiber tracking. This study investigates whether HARDI fiber tracking can be used to robustly delineate the full extent of the tract.

Materials and Methods—HARDI (64-direction, $b=3000$ s/mm²) and DTI (30-direction, $b=1000$ s/mm²) were acquired from 25 control subjects between the ages of 8 and 26 years. Probabilistic HARDI and DTI fiber tracking of the auditory radiation was performed with starting and filter regions automatically generated from the freesurfer white matter parcellation. DTI fiber tracking was performed with both the 64 and 30-direction data sets. Fiber tracking trials demonstrating connectivity from Heschl's gyrus to the medial geniculate nucleus were considered successful.

Results—HARDI fiber tracking success rate was 98% and significantly higher than the 64-direction DTI rate of 50% or the 30-direction DTI rate of 42% ($p<0.001$). The success rates of HARDI fiber tracking for the left and right auditory radiations were not significantly different. In contrast, the left auditory radiation was successfully delineated with DTI fiber tracking at a higher rate than the right auditory radiation.

Conclusions—HARDI can discriminate the complex white matter pathways at the junction of the auditory radiation and the inferior longitudinal fasciculus. HARDI fiber tracking can reliably delineate the auditory radiation.

Introduction

Diffusion MR fiber tracking uses the random motion of water to determine the orientation of coherent axonal bundles^{1,2}. In particular, fiber tracking follows the estimated fiber orientation voxel to voxel in 3D to delineate specific white matter pathways³⁻⁶. Diffusion tensor imaging (DTI) fiber tracking has become a standard tool for analyzing white matter tract geometry and microstructure. DTI fiber tracking software is readily available from

Address for Correspondence: Jeffrey I. Berman, PhD Dept. of Radiology Children's Hospital of Philadelphia Wood Bldg, Suite 2115 34th and Civic Center Blvd. Philadelphia, PA 19104 Tel: 267-426-2988 bermanj@email.chop.edu.

This work has in part been presented as an abstract to ISMRM.

research groups and MR scanner manufacturers. Accordingly, there has been a surge in the number of publications using DTI fiber tracking to delineate specific tracts for qualitative or quantitative purposes. A limitation, however, is that the diffusion tensor model fails to accurately represent the complex architecture of crossing white matter fibers. For this reason, DTI fiber tracking fails to accurately follow white matter pathways through tract intersections.

High angular resolution diffusion imaging (HARDI) is capable of discriminating multiple fiber populations crossing within the same voxel. HARDI requires the acquisition of over 50 gradient directions at high b-value, while DTI only requires 6 directions at lower b-values. The higher angular resolution provides a more accurate representation of the 3D pattern of water diffusion within a voxel. Numerous methods exist to reconstruct the architecture of brain tissue from HARDI data⁷⁻¹². All methods have in common the ability to provide the orientation of multiple white matter tracts within each voxel. Fiber tracking with HARDI can follow white matter tracts through regions of crossing fibers whereas DTI fiber tracking would terminate or provide erroneous results in these same areas¹³⁻¹⁶.

The auditory radiations are an important sensory pathway which relays acoustic information from the medial geniculate nucleus of the thalamus to primary auditory cortex. The auditory radiation crosses the inferior longitudinal fasciculus, a major anterior-posterior white matter tract. Thus, DTI fiber tracking cannot consistently delineate the auditory radiation. In a prior study, probabilistic DTI fiber tracking was capable of following the acoustic pathway from the cortex to the inferior colliculus in only 50% of trials¹⁷. This study compares the performance of probabilistic HARDI to probabilistic DTI fiber tracking of the auditory radiation. The goal of this study is to develop a robust framework for studying a primary sensory pathway that is often difficult to identify using traditional quantitative measurement methods.

Methods

MR Imaging

MR imaging was performed with a 3T Siemens Verio™ (Siemens Medical Solutions, Erlangen, Germany) scanner on 25 children and adults between the ages of 8 and 26 years (mean age 16.4 years). All subjects were healthy volunteers and had no abnormal finding on MRI. Informed consent was obtained from each subject or their guardian as applicable according to our institution's regulations. The whole-brain HARDI acquisition included 64 gradient directions at $b=3000 \text{ s/mm}^2$, $TR/TE=14.8\text{s}/111\text{ms}$, voxel size= $2\times 2\times 2\text{mm}$, and 128×128 matrix. Two $b=0 \text{ s/mm}^2$ volumes are included in the HARDI acquisition. An additional DTI acquisition used 30 diffusion gradient directions at $b=1000 \text{ s/mm}^2$, one $b=0 \text{ s/mm}^2$ volume, $TR/TE=11\text{s}/76\text{ms}$, voxel size $2\times 2\times 2\text{mm}$, and 128×128 matrix. The 30-direction diffusion sequence is the routine clinical DTI sequence used at our institution. The HARDI acquisition was approximately 18 minutes in duration and the DTI acquisition 6 minutes in duration. Both HARDI and DTI acquisitions used a Stejskal-Tanner monopolar, spin-echo echo planar sequence, a 32-channel head coil, maximum gradient strength of 45 mT/m, and parallel acceleration factor of 2 with GRAPPA (Siemens, Erlangen, Germany). Diffusion volumes were corrected for eddy current distortion with the Oxford Centre for

Functional MRI of the Brain Diffusion Toolbox in FSL¹⁸. Anatomical T1-weighted MP-RAGE volumes were also acquired from each subject with TR/TE=2000/3.71 ms, 1mm isotropic voxels, and full head coverage.

Diffusion MR Fiber Tracking

The solid angle q-ball reconstruction of the HARDI data was used with a probabilistic fiber tracking algorithm^{8, 13}. The HARDI fiber tracking algorithm uses the residual bootstrap to estimate the uncertainty in the q-ball fiber orientation estimates. The range of probable fiber orientations is probed with a Monte Carlo strategy as each voxel is visited many times by independent tracks. The total number of fiber trajectories passing through each voxel provides a confidence level of that voxel's inclusion in the tract of interest. For comparison, probabilistic DTI fiber tracking was performed with both the 64 diffusion gradient direction HARDI acquisition and the 30 direction standard DTI acquisition. The DTI fiber tracking algorithm uses the residual bootstrap to estimate uncertainty in the primary eigenvector orientation¹⁹. The DTI and HARDI fiber tracking probabilistic algorithms utilize similar statistical methods to estimate uncertainty and propagate fiber trajectories. A Monte Carlo strategy probes the range of possible propagation directions, and trajectories are based upon fiber assignment by continuous tracking (FACT)⁴. Both HARDI and DTI fiber tracking were implemented with in-house software written in Interactive Data Language (Exelis Visual Solutions, Boulder, CO).

Volume segmentation and white matter parcellation was performed with Freesurfer on each subject's T1-weighted image and used to generate regions of interest for fiber tracking²⁰. The T1-weighted volume was registered with FMRIB's Linear Image Registration Tool (FLIRT) to the echo planar volumes without diffusion weighting (b=0) from the 30 direction and 64 direction diffusion acquisitions²¹. The two b=0 volumes from the 64 direction acquisition were averaged prior to registration. All registrations were visually examined to ensure correct placement of major sulci and ventricles. The Freesurfer parcellation map was then mapped into the coordinate space of each diffusion acquisition. The white matter of the transverse temporal gyrus was used to launch fiber tracks. A target region including the medial geniculate nucleus was generated with custom-built software operating on the freesurfer parcellations. The thalamus and ventral diencephalon segmentations were first dilated with a 2×2×2 voxel structuring element. The intersection of the two dilated segmentations is on the inferior surface of the thalamus and is retained as the target region of interest. Figure 1 shows the starting and target regions. A set of regions of interest outside the auditory radiation were used to eliminate common patterns of errant fiber trajectories. These additional regions included the medial orbitofrontal white matter, corpus callosum, isthmus of the cingulate gyrus, precentral gyrus, supramarginal gyrus, putamen, and pallidum. Fiber tracks passing through the starting and target regions but not the exclusion regions were retained as the auditory radiation.

HARDI and DTI fiber tracking were each performed with an FA threshold of 0.125, an angle threshold of 70°, and 128 starting points per voxel. A low FA threshold was chosen because HARDI can detect fiber architecture in voxels where the diffusion tensor model

produces low FA. The relatively high angle threshold reflects the ability of HARDI to detect crossing fibers. Tractography was performed at the native 2×2×2mm image resolution.

Successful fiber tracking was defined as the presence of at least one trajectory connecting Heschl's gyrus to the medial geniculate nucleus. To further examine performance, the number of trajectories produced by each fiber tracking method was compared by adjusting the threshold for successful fiber tracking. Left and right side auditory radiations were examined separately. Comparisons between rates of success were performed with McNemar's Chi-square test.

Results

Figure 2 shows an example set of HARDI fiber tracks (red streamlines), following the auditory radiation from the auditory cortex (AC) to the thalamus. The q-ball orientation density functions show the anterior-posterior ILF (green peaks) crossing the smaller left-right peaks of the auditory radiation. The HARDI fiber tracking follows the auditory radiation through the crossing, whereas DTI fiber tracking fails. Figure 3 shows DTI fiber tracks emerging from Heschl's gyrus and incorrectly following the dominant anterior-posterior coursing ILF.

At a threshold of one trajectory, the success rate of HARDI fiber tracking was 98%, 64-direction DTI 50%, and 30-direction DTI 42%. HARDI fiber tracking successfully delineated the auditory radiation at a significantly higher rate than either DTI fiber tracking method (McNemar Chi-Square Test with Bonferroni correction, $p < 0.001$ each, Table 1). The success rate of 30-direction low b-value and 64-direction high b-value DTI fiber tracking were not significantly different. Age was not correlated with fiber tracking success for any fiber tracking method (Logistic regression, $p > 0.4$ for each).

The success rates of HARDI fiber tracking for the left and right auditory radiations were not significantly different. In contrast, the left auditory radiation was successfully delineated with DTI fiber tracking at a higher rate than the right auditory radiation. This hemisphere difference was significant for both 30-direction and 64-direction DTI fiber tracking ($p < 0.003$ each, McNemar Chi-Square Test with Bonferroni correction, Table 1).

Figure 5 examines fiber tracking results as the number of trajectories threshold is varied from 1 to 200. DTI and HARDI rates of success decrease as the threshold is increased. However, the HARDI rate of success is significantly higher than the 30-direction DTI success rate through a threshold of 10 and the 64-direction DTI success rate through a threshold of 20 ($p < 0.01$ each, McNemar Chi-Square Test).

Discussion

This study demonstrates the advantage of using HARDI to perform fiber tracking of the auditory radiation. HARDI can reliably resolve crossing white matter tracts at the intersection of the auditory radiation and the ILF. In contrast, the diffusion tensor model often fails to accurately represent the microstructure at this junction and only depicts the orientation of the dominant ILF tract. The DTI fiber tracking success rate observed in this

study is consistent with the results from Crippa, et. al¹⁷. DTI fiber tracking performance with the 64 direction ($b=3000s/mm^2$) diffusion data was not significantly different than the 30 direction ($b=1000s/mm^2$) data, with neither robustly successful. Present results thus indicate that improved signal-to-noise ratio or increased number of directions cannot improve DTI fiber tracking performance.

The HARDI acquisition is longer than a traditional DTI acquisition however it has been successfully included in our pediatric and adult research protocols. In terms of implementing HARDI, the primary differences between a DTI and HARDI acquisition are the number of directions and the b-value. Changing these parameters is straightforward on many scanners, however higher b-values produce images with lower SNR. High-field strength and high specification gradients are necessary to improve SNR at high b-values. A current limitation is that HARDI post-processing is not a feature available on most scanners. However, as HARDI is translated into a clinical tool, the availability of HARDI reconstruction algorithms and fiber tracking tools is expected to improve.

Diffusion MR and tractography provide an estimate of white matter microstructure and connectivity^{22, 23}. Tractography operates under the assumption that white matter fiber orientation can be inferred from the random movement of water. The choice of image acquisition parameters and tractography algorithm determines the accuracy of tractography results. Image noise, low spatial resolution, and low number of diffusion gradient directions are imaging factors which limit the accuracy of calculated fiber orientations. When incorrect HARDI or DTI fiber orientations are used for tractography, errors propagate along the trajectories. A non-invasive gold standard for the subcortical position of the auditory radiation does not exist. However, prior knowledge of neuroanatomy can be added by the user to delineate a specific tract. This study used multiple atlas based starting, target, and filter regions of interest to constrain the fiber tracks to the auditory radiation.

Probabilistic algorithms attempt to compensate for noise and inherent inaccuracies of the HARDI and DTI methods by probing multiple possible propagation directions. Deterministic fiber tracking algorithms are common, but they do not account for the uncertainty inherent in all diffusion MR experiments. The probabilistic fiber tracking algorithms used in this study estimate the uncertainty in the HARDI and DTI fiber orientations with the bootstrap method^{13, 19, 24, 25}. The residual bootstrap technique is a method of determining the probability distribution of fiber orientations from one diffusion MR acquisition. It is necessary to launch a large number of trajectories from the starting region to probe the range of possible fiber orientations along the tract. The number of fiber trajectories passing through a voxel provides a relative assessment of that voxel's likelihood of inclusion in the tract of interest. However, there is no way to translate the number of trajectories to an absolute metric of probability. The number of trajectories generated is related to the size of the starting region and the density of starting points. As seen in figure 5, HARDI ceased to perform better than DTI at a threshold of 20 trajectories. However, this threshold level is directly related to the number of starting points.

Prior quantitative studies of the auditory radiation have relied upon region of interest measurements within the tract. Lutz et. al. placed regions of interest in Heschl's gyrus and

the acoustic radiation adjacent to the thalamus to study the effect of aging on the auditory system²⁶. Roberts et al. used regions of interest in Heschl's gyrus to measure the correlation of diffusion anisotropy (based on DTI) to MEG-detected electrophysiologic auditory evoked superior temporal gyrus responses²⁷. Manually placed regions of interest are restricted to points within the auditory radiation near known landmarks. Hand drawn region of interest measurements have higher variability than measures originating from 3D regions of interest defined by fiber tracking²⁸. In addition, white matter tracts have heterogeneous geometry and microstructure as they course through different regions of the cerebrum. Regions of interest which only outline a small portion of the tract may not be representative of the entire tract or be sensitive to microstructural changes occurring elsewhere along the tract. As shown in the present study, HARDI fiber tracking extends the localization of auditory radiation tracts beyond the landmarks used as starting and target regions. Thus, this work provides the framework for quantitative studies of the entire auditory radiation.

DTI fiber tracking was more successful in delineating the left auditory radiation than the right. This asymmetry may be attributed to the structural and functional asymmetries of the language and auditory systems²⁹⁻³². Greater left-hemisphere cortical activity and white matter volumes in language networks may be related to a larger and more compact auditory radiation. In addition, diffusion fiber tracking studies have shown structural asymmetry in the ILF^{33, 34}. These factors reduce DTI partial voluming and increase diffusion anisotropy. These structural differences may result in an improved success rate of DTI fiber tracking of the left auditory radiation. However, HARDI fiber tracking demonstrated no asymmetry in performance because of its ability to discriminate crossing fibers in both hemispheres.

The auditory radiation is a primary sensory pathway and is important for language comprehension. Auditory dysfunction measured with magnetoencephalography has been associated with autism spectrum disorders³⁵. Abnormal morphology and diffusion parameters in Heschl's gyrus have been identified in schizophrenia^{36, 37}. Further studies are needed to investigate the microstructure of the auditory radiation in these neuropsychiatric disorders. This study's findings indicate that more detailed and robust measures of the auditory radiation can be obtained using HARDI fiber tracking. Unlike other primary sensory pathways such as somatosensory and optic radiations, HARDI is necessary for study of the acoustic radiation because traditional DTI fiber tracking analysis is not reliable in this tract. HARDI metrics that describe tract-specific microstructure are still under development. In the future, these HARDI metrics may be combined with HARDI fiber tracking to perform microstructural assessment of the auditory radiation in clinical studies.

Conclusion

HARDI fiber tracking of the auditory radiation performs significantly better than DTI fiber tracking, with HARDI easily discriminating the complex white matter pathways at the junction of the auditory radiation and the ILF. HARDI is thus a necessary component of clinical studies seeking to assess the entire auditory radiation with diffusion MR.

Acknowledgments

This study was supported in part by NIH grant R01DC008871 (TR), NIH grant R01DC008871-02S1, a NIH grant K01MH096091 (JIB), a NIH grant K08 MH085100 (JCE), and Award P30HD026979 from the Eunice Kennedy Shriver National Institute of Child Health & Human Development of the NIH. Additional grants were from the Research Scientist Award of the Foundation for the ASNR, the Nancy Lurie Marks Family Foundation (NLMFF) and Autism Speaks. This research has been funded in part by a grant from the Pennsylvania Department of Health. The Pennsylvania Department of Health specifically disclaims responsibility for any analyses, interpretations or conclusions. The authors gratefully acknowledge Thorsten Feiweier of Siemens for providing the diffusion works in progress pulse sequence used in this work.

Abbreviations

AC	Auditory cortex
DTI	Diffusion tensor imaging
FACT	Fiber Assignment by Continuous Tracking
FMRIB	Oxford Center for Functional MRI of the Brain
FSL	Functional MRI of the Brain Software Library
GRAPPA	Generalized Autocalibrating Partially Parallel Acquisition
HARDI	High angular resolution diffusion imaging
ILF	Inferior longitudinal fasciculus
MEG	Magnetoencephalography
MP-RAGE	Magnetization-Prepared Rapid Acquisition with Gradient Echo
MRI	Magnetic resonance imaging
SNR	Signal to Noise Ratio
TE	Echo Time
TR	Repetition Time

References

1. Basser PJ, Mattiello J, LeBihan D. Estimation of the effective self-diffusion tensor from the NMR spin echo. *J Magn Reson B*. 1994; 103:247–54. [PubMed: 8019776]
2. Beaulieu C. The basis of anisotropic water diffusion in the nervous system - a technical review. *NMR Biomed*. 2002; 15:435–55. [PubMed: 12489094]
3. Conturo TE, Lori NF, Cull TS, et al. Tracking neuronal fiber pathways in the living human brain. *Proc Natl Acad Sci USA*. 1999; 96:10422–7. [PubMed: 10468624]
4. Mori S, Crain BJ, Chacko VP, et al. Three-dimensional tracking of axonal projections in the brain by magnetic resonance imaging. *Ann Neurol*. 1999; 45:265–9. [PubMed: 9989633]
5. Mori S, van Zijl PC. Fiber tracking: Principles and strategies - a technical review. *NMR Biomed*. 2002; 15:468–80. [PubMed: 12489096]
6. Basser PJ, Pajevic S, Pierpaoli C, et al. In vivo fiber tractography using DT-MRI data. *Magn Reson Med*. 2000; 44:625–32. [PubMed: 11025519]
7. Tuch DS. Q-ball imaging. *Magn Reson Med*. 2004; 52:1358–72. [PubMed: 15562495]
8. Aganj I, Lenglet C, Sapiro G, et al. Reconstruction of the orientation distribution function in single- and multiple-shell q-ball imaging within constant solid angle. *Magn Reson Med*. 2010; 64:554–66. [PubMed: 20535807]

9. Tournier J- Yeh C, Calamante F, et al. Resolving crossing fibres using constrained spherical deconvolution: Validation using diffusion-weighted imaging phantom data. *Neuroimage*. 2008; 42:617–25. [PubMed: 18583153]
10. Hess CP, Mukherjee P, Han ET, et al. Q-ball reconstruction of multimodal fiber orientations using the spherical harmonic basis. *Magn Reson Med*. 2006; 56:104–17. [PubMed: 16755539]
11. Tournier JD, Calamante F, Gadian DG, et al. Direct estimation of the fiber orientation density function from diffusion-weighted MRI data using spherical deconvolution. *Neuroimage*. 2004; 23:1176–85. [PubMed: 15528117]
12. Özarslan E, Shepherd TM, Vemuri BC, et al. Resolution of complex tissue microarchitecture using the diffusion orientation transform (DOT). *Neuroimage*. 2006; 31:1086–103. [PubMed: 16546404]
13. Berman, JI; Chung, S.; Mukherjee, P., et al. Probabilistic streamline Q-ball tractography using the residual bootstrap. *Neuroimage*. 2008; 39:215–22. [PubMed: 17911030]
14. Perrin M, Poupon C, Cointepas Y, et al. Fiber tracking in q-ball fields using regularized particle trajectories. *Inf Process Med Imaging*. 2005; 19:52–63. [PubMed: 17354684]
15. Campbell JS, Siddiqi K, Rymar W, et al. Flow-based fiber tracking with diffusion tensor and q-ball data: Validation and comparison to principal diffusion direction techniques. *Neuroimage*. 2005; 27:725–36. [PubMed: 16111897]
16. Behrens TE, Berg HJ, Jbabdi S, et al. Probabilistic diffusion tractography with multiple fibre orientations: What can we gain? *Neuroimage*. 2007; 34:144–55. [PubMed: 17070705]
17. Crippa A, Lanting CP, van Dijk P, et al. A diffusion tensor imaging study on the auditory system and tinnitus. *Open Neuroimag J*. 2010; 4:16–25. [PubMed: 20922048]
18. Smith SM, Jenkinson M, Woolrich MW, et al. Advances in functional and structural MR image analysis and implementation as FSL. *Neuroimage*. 2004; 23(Suppl 1):S208–19. [PubMed: 15501092]
19. Chung S, Lu Y, Henry RG. Comparison of bootstrap approaches for estimation of uncertainties of DTI parameters. *Neuroimage*. 2006; 33:531–41. [PubMed: 16938472]
20. Fischl B, Sereno MI, Tootell RB, et al. High-resolution intersubject averaging and a coordinate system for the cortical surface. *Hum Brain Mapp*. 1999; 8:272–84. [PubMed: 10619420]
21. Jenkinson M, Smith S. A global optimisation method for robust affine registration of brain images. *Medical Image Analysis*. 2001; 5:143–56. [PubMed: 11516708]
22. Chung HW, Chou MC, Chen CY. Principles and limitations of computational algorithms in clinical diffusion tensor MR tractography. *Am J Neuroradiol*. 2011; 32:3–13. [PubMed: 20299436]
23. Mori S, van Zijl P. Fiber tracking: Principles and strategies – a technical review. *NMR Biomed*. 2008; 15:468–80. [PubMed: 12489096]
24. Jones DK, Pierpaoli C. Confidence mapping in diffusion tensor magnetic resonance imaging tractography using a bootstrap approach. *Magn Reson Med*. 2005; 53:1143–9. [PubMed: 15844149]
25. Jeurissen B, Leemans A, Jones DK, et al. Probabilistic fiber tracking using the residual bootstrap with constrained spherical deconvolution. *Human Brain Mapping*. 2011; 32:461–79. [PubMed: 21319270]
26. Lutz J, Hemminger F, Stahl R, et al. Evidence of subcortical and cortical aging of the acoustic pathway: A diffusion tensor imaging (DTI) study. *Acad Radiol*. 2007; 14:692–700. [PubMed: 17502259]
27. Roberts TPL, Khan SY, Blaskey L, et al. Developmental correlation of diffusion anisotropy with auditory-evoked response. *Neuroreport*. 2009; 20:1586–91. [PubMed: 19898261]
28. Partridge SC, Vigneron DB, Charlton NN, et al. Pyramidal tract maturation after brain injury in newborns with heart disease. *Ann Neurol*. 2006; 59:640–51. [PubMed: 16450369]
29. Morillon B, Lehongre K, Frackowiak RS, et al. Neurophysiological origin of human brain asymmetry for speech and language. *Proc Natl Acad Sci U S A*. 2010; 107:18688–93. [PubMed: 20956297]
30. Devlin JT, Raley J, Tunbridge E, et al. Functional asymmetry for auditory processing in human primary auditory cortex. *J Neurosci*. 2003; 23:11516–22. [PubMed: 14684855]

31. Ackermann H, Hertrich I, Mathiak K, et al. Contralaterality of cortical auditory processing at the level of the M50/M100 complex and the mismatch field: A whole-head magnetoencephalography study. *Neuroreport*. 2001; 12:1683–7. [PubMed: 11409739]
32. Geschwind N, Levitsky W. Human brain: Left-right asymmetries in temporal speech region. *Science*. 1968; 161:186–7. [PubMed: 5657070]
33. Wakana S, Caprihan A, Panzenboeck MM, et al. Reproducibility of quantitative tractography methods applied to cerebral white matter. *Neuroimage*. 2007; 36:630–44. [PubMed: 17481925]
34. Thiebaut de Schotten M, Ffytche DH, Bizzi A, et al. Atlasing location, asymmetry and inter-subject variability of white matter tracts in the human brain with MR diffusion tractography. *Neuroimage*. 2011; 54:49–59. [PubMed: 20682348]
35. Roberts TPL, Khan SY, Rey M, et al. MEG detection of delayed auditory evoked responses in autism spectrum disorders: Towards an imaging biomarker for autism. *Autism Research*. 2010; 3:8–18. [PubMed: 20063319]
36. Douaud G, Smith S, Jenkinson M, et al. Anatomically related grey and white matter abnormalities in adolescent-onset schizophrenia. *Brain*. 2007; 130:2375–86. [PubMed: 17698497]
37. Lee K, Yoshida T, Kubicki M, et al. Increased diffusivity in superior temporal gyrus in patients with schizophrenia: A diffusion tensor imaging study. *Schizophr Res*. 2009; 108:33–40. [PubMed: 19135872]

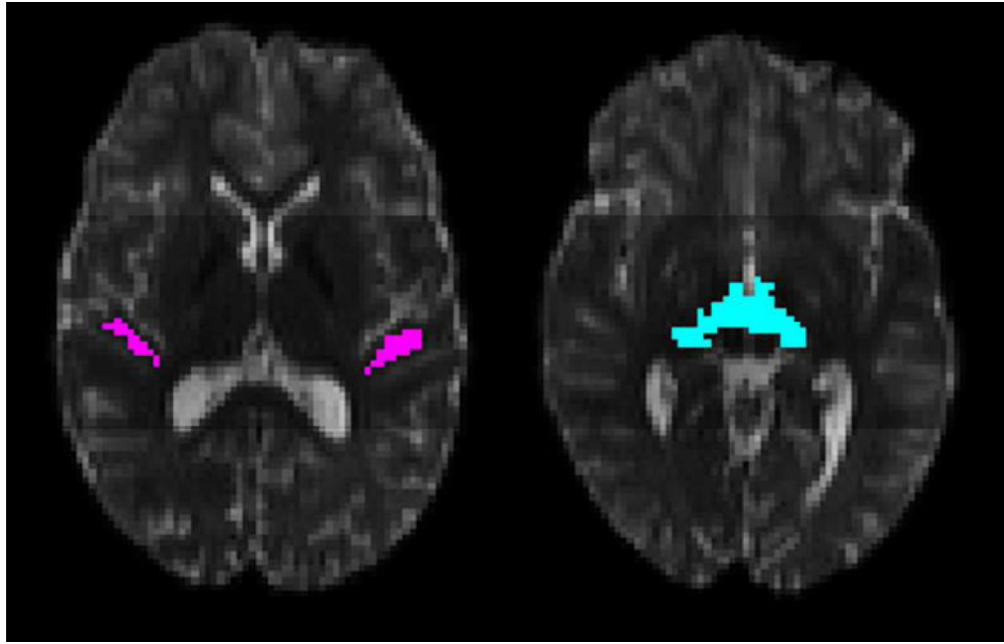


Figure 1. The starting region of interest for fiber tracking within Heschl's gyrus is shown on the left. The target region of interest on the inferior surface of the thalamus is shown on the right. The regions are shown overlaid on axial slices through the $b=0$ s/mm² echo planar volume from the 64-direction HARDI acquisition.

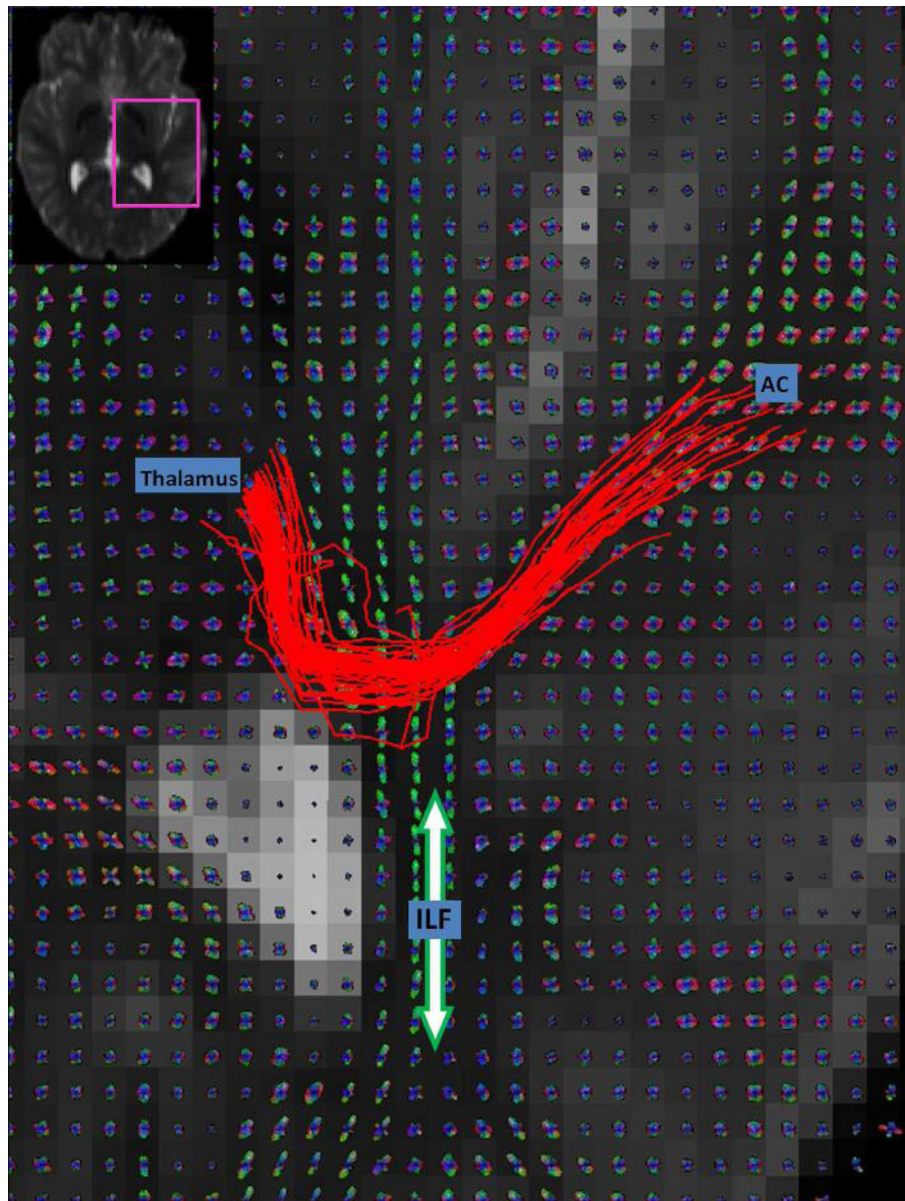


Figure 2. Q-ball reconstructions of the HARDI data are shown for each voxel on an axial slice. HARDI fiber tracks (red streamlines) course from the auditory cortex to the thalamus. The inferior longitudinal fasciculus (ILF, green fiber peaks and orientation indicated with arrow) intersects the auditory radiation.

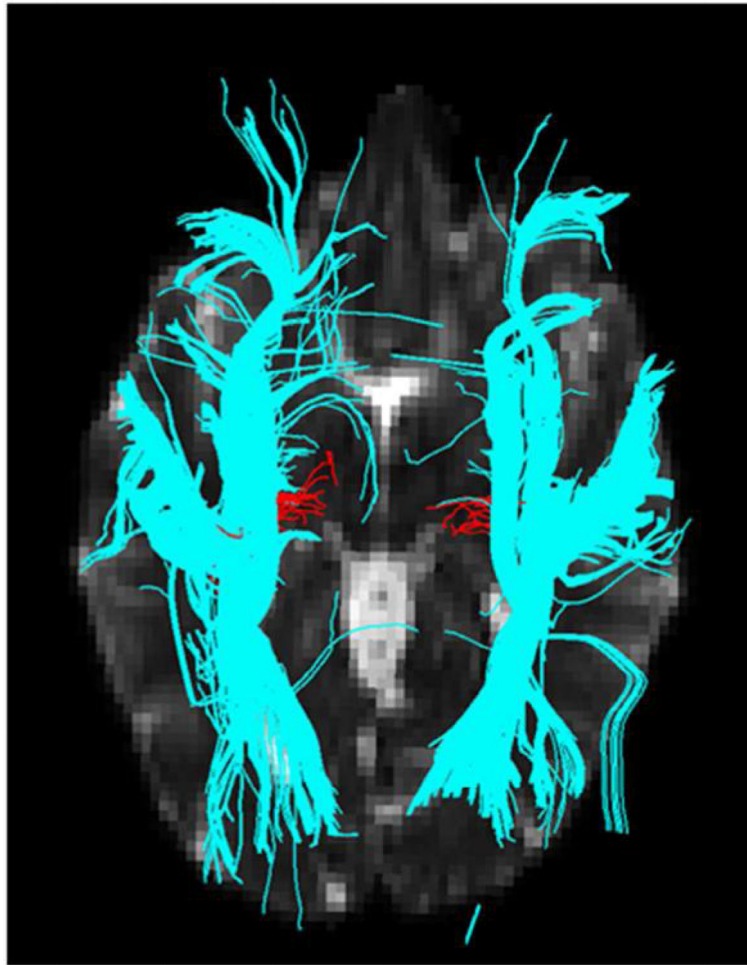


Figure 3.

HARDI fiber tracks (red) and DTI fiber tracks (blue) are visualized in the left and right hemispheres. DTI fiber tracks are from the 64-direction dataset. The left hemisphere is on the left side of the figure. Both HARDI and DTI fiber tracks were launched from the same starting regions in Heschl's gyrus. The HARDI fiber tracks reaching the thalamic target regions are retained. For this figure, all DTI fiber tracks are retained, regardless of destination. The DTI fiber tracks emerge from Heschl's gyrus and follow the inferior longitudinal fasciculus in either the anterior or posterior direction. No DTI fiber tracks cross the ILF to reach the thalamus in the right hemisphere.

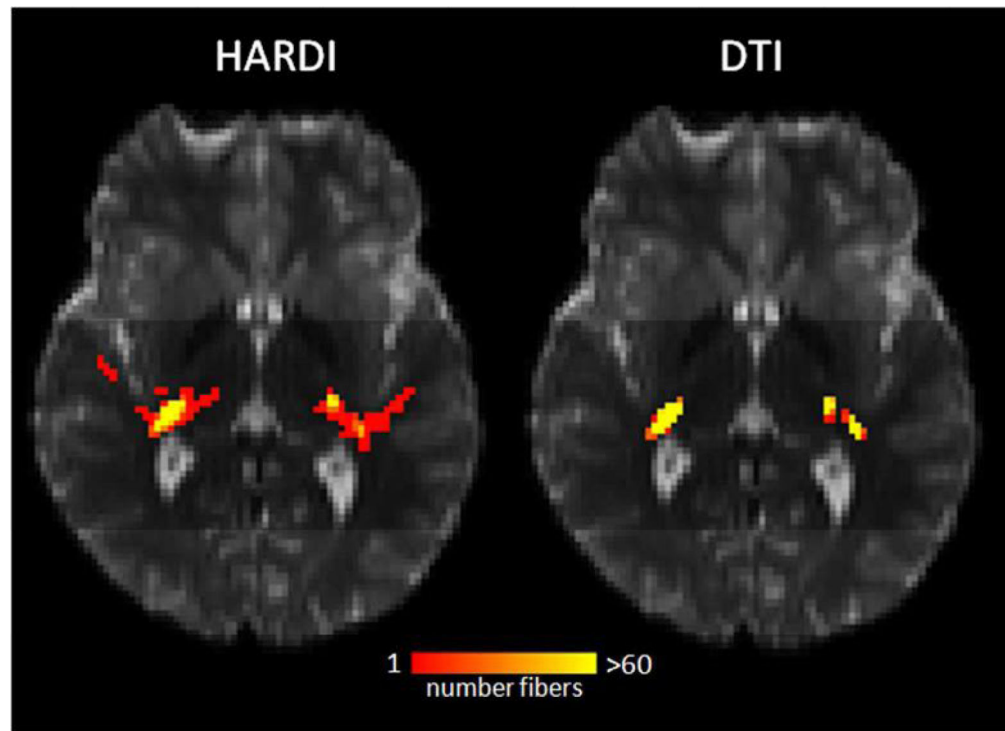


Figure 4. HARDI and DTI fiber tracks connecting the auditory cortex to the thalamus target region are shown in a case where both methods were successful in each hemisphere. The number of fiber trajectories passing through each voxel is encoded with the overlay color. The yellow voxels have the highest probability of being within the auditory radiation.

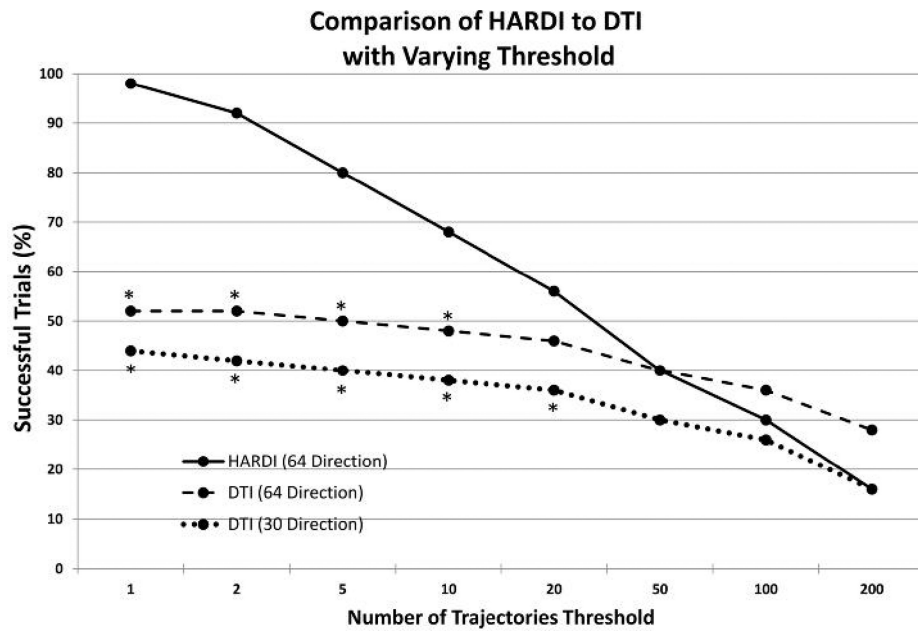


Figure 5. The threshold for successful fiber tracking is varied between 1 and 200 trajectories connecting the auditory cortex to the thalamus. The percent of successful HARDI and DTI fiber tracking trials is shown at each threshold. An asterisk indicates the HARDI rate of success is significantly higher than the respective DTI fiber tracking rate of success ($p < 0.01$).

Table 1

Comparison of DTI and HARDI auditory fiber tracking results. Successful connections contained one or more fiber trajectories.

	Successful			Unsuccessful		
	Left	Right	Total	Left	Right	Total
DTI – 30 Directions	16	5	21	9	20	29
DTI – 64 Directions	18	7	25	7	18	25
HARDI – 64 Directions	24	25	49	1	0	1